# We are IntechOpen, the world's leading publisher of Open Access books Built by scientists, for scientists

**4,800**
Open access books available

**122,000**
International authors and editors

**135M**
Downloads

Our authors are among the

**154**
Countries delivered to

**TOP 1%**
most cited scientists

**12.2%**
Contributors from top 500 universities

CLARIVATE ANALYTICS BOOK CITATION INDEX INDEXED

WEB OF SCIENCE™

Selection of our books indexed in the Book Citation Index in Web of Science™ Core Collection (BKCI)

## Interested in publishing with us?
## Contact book.department@intechopen.com

Numbers displayed above are based on latest data collected.
For more information visit www.intechopen.com

# 6

# Solar Energy Absorbers

Himanshu Dehra
*Noise Behaviour Institute, McGill University*
*Department of Public Health Medicine, McGill University*
*Energy Management Research Centre, McGill University*
*Department of Mining Engineering, McGill University*
*Department of Building Engineering, Concordia University*
*Centre for Building Studies, Concordia University*
*Concordia Institute of Information Systems Engineering, Concordia University*
*Département de Communication Sociale et Publique, UQÀM*
*Akal Takht (1-140 Avenue Windsor, Lachine, Québec)*
*Concordia*

## 1. Introduction

The most of the solar energy is absorbed by moving planets, their satellites and their surrounding environment viz., planet surface, planet atmosphere, forests, farms, rivers, ponds, lakes & seas, living beings and civil structures (e.g. buildings, green houses, thermal power plants, collectors, panels, roads, bridges, ports, canals). The life and its activities are reliant upon the sun's radiant energy which apart from the earth is also stocked up by green plants. In addition to the primary role of light in living economy, a continual environment of mixed radiations from various sources of radiations produce other effects, reactions and adaptations, which have susceptibility to influence the life activities of the living organisms living in a continual environment. The solar radiation is passed through the earth's atmosphere and while passing, the solar radiation is reflected, scattered, and absorbed by gas molecules, ozone, water vapour, clouds and dust. The length of atmospheric path travel by sun rays is determined by the air mass $m$, the ratio of the mass of atmosphere in the actual earth-sun path to the mass which would exist if the sun were directly overhead at sea level ($m$=1.0).

The sunlight is the major source of radiations on the earth. The spectrum of sunlight includes ultraviolet radiation, visible light, infrared rays and radio waves. The x-rays are generated by solar flares and their ionization due to absorption occurs high in the earth's atmosphere. X-rays also reach the earth's atmosphere from various celestial sources. About 60 per cent of the energy of sunlight is in the invisible infrared region's indefinite limit in radiation spectrum of sunlight. The sunlight radiations of shorter wavelengths are absorbed in the earth's atmosphere before such radiations reach the surface of earth. The ozone layer is formed high above the atmosphere through absorption of ultraviolet radiation by oxygen. The reversible reaction, again turn the ozone to absorbs longer ultraviolet rays, re-forming oxygen. The radioactive emanations consist of three components: i) gamma rays, which are penetrating radiations of very short wavelength but otherwise like x-rays; ii) alpha particles,

positively charged helium nuclei; and iii) beta particles, rapidly moving electrons. The artificial radioactive elements are formed by bombardment with high energy particles such as helium nuclei. The most of the radiation in ultraviolet region of radiation spectrum is absorbed by the ozone in the upper atmosphere, whilst part of the radiation in the shortwave region of the radiation spectrum is scattered by air molecules, for communication of blue colour appearance of sky to our eyes. The strength of the absorption of solar energy varies with wavelength and absorption bands are formed at regions of strong absorption. The important atmospheric gases forming part of absorption bands are ozone ($O_3$), water vapour ($H_2O$), carbon dioxide ($CO_2$), oxygen ($O_2$), methane ($CH_4$), chlorofluorocarbons (CFC) and nitrogen dioxide ($NO_2$).

The scope of the chapter is to present detailed theoretical aspects of solar energy absorbers, their radiation properties, radiation sources, diffraction and measurement of radiation sources. The importance of selection of roughness factors based on fluid flow is pointed out. The human environmental health is presented for metabolism of your body to intense solar radiation and heat. Mathematical analysis of a solar thermosyphon and experimental results for applications of solar collectors to the environment, human health and buildings are elaborated later in the chapter.

## 2. Theory

The rate of electromagnetic radiation emitted at a rate $E_x$ from the surface of a solar energy absorber is given by the Stefan-Boltzmann equation as follows:

$$E_x = \varepsilon\sigma T^4 \tag{1}$$

Where, $E_x$ is exitance of a solar energy absorber, T is temperature in K, σ is Stefan-Boltzmann constant, 5.67 x $10^8$ W/($m^2$.$K^4$) and ε is hemispherical emittance for a surface of solar energy absorber. The theoretical maximum value of hemispherical emittance possible from the surface of a solar energy absorber is 1.0. The radiation emitted from the surface of a solar energy absorber for ε=1.0, at normal emittance is called blackbody radiation.

Measurement of Radiation: The intensity of all radiation is measured in terms of amounts of energy per unit time per unit area. When radiation is measured in terms of its heating power, it is only necessary to absorb all the incident radiation on a black surface and convert the radiation to heat which may be taken up in water and measured by a thermometer as in heliometers used for measuring the energy of sunlight. The small amount of radiation is measured by placement of thermocouples in water or on the black receiving surface.

### 2.1 Radiation properties

Source and Sink: A line normal to the plane, from which energy is imagined to flow uniformly in all directions at right angles to it, is a source. It appears as a point in the customary two-dimensional energy flow diagram. The total energy flow per unit time and unit length of line is called the strength of the source. As the flow is in radial lines from the source, the current of energy flow is at a distance r from the source, which is determined by the strength divided by the energy flow area.

The radiation of the sun, direct rays from the sun and diffuse rays from the sky, clouds, and surrounding objects incident on a transparent surface of a solar energy absorber is partly transmitted and partly reflected. In addition to this some part of the radiation is absorbed by

the selective coating on the surface of a solar energy absorber. The part of the incident flux that is reflected is called the reflectance ρ, the part absorbed is called the absorptance α, and the part transmitted is called the transmittance τ. The sum of reflectance, absorptance and transmittance is unity, or

$$\rho + \alpha + \tau = 1 \tag{2}$$

The radiation incident on the surface of a solar energy absorber has non-constant distributions over the directions of incidence and over the wavelength (or frequency) scale. The radiation properties transmittance, reflectance and absorptance are properties of a specific thickness for a sample of selective material of a solar energy absorber. The emittance ε of the surface of a solar energy absorber is the ratio of the emission of thermal radiant flux from a surface to the flux that would be emitted by a blackbody emitter at the same temperature. The angular dependence for radiation properties is explained through a solid angle formed by all rays joining a point to a closed curve. For a sphere of radius R, the solid angle is the ratio of the projected area A on the sphere to the square of length R. A sphere has a solid angle of 4 π steradians. The solar radiation incident on a point at a surface of a solar energy absorber comes from many directions in a conical solid angle. For a cone of half angle θ, the solid angle defined by the circular top and point bottom of that cone is given by

$$\Omega = 2\,\pi\,(1-\cos\theta) \tag{3}$$

In measurement of the transmittance or reflectance, a sample is illuminated over a specified solid angle. The flux is then collected for a given solid angle to measure reflectance or transmittance. A conical solid angle is bound by right circular cone. The source of solar radiation is sunlight. The radiation properties of sunlight necessary for performance analysis of daylighting and lighting are defined as follows:

The luminous flux is the time rate of flow of light. A receiver surface of a solar energy absorber receives watts of sunlight and it emits luminous flux. The measure of the rate of success in converting watts of sunlight to lumens is called efficacy.

The illuminance on a surface of a solar energy absorber is the density of luminous flux incident on that surface. The luminous flux travels outward from a source, it ultimately impinges on many surfaces, where it is reflected, transmitted and absorbed.

Luminous intensity is the force generating the luminous flux. A source of sunlight is described as having a luminous intensity in a particular direction. The inverse square law of illumination states that the illuminance on a surface perpendicular to the line from the point source of sunlight to the surface of a solar energy absorber varies directly with the intensity of the source and inversely with the square of the distance from the source of sunlight to the surface of a solar energy absorber.

The luminance of a source or a sink is defined as the intensity of the source or the sink in the direction of an observer divided by the projected area of the source or sink as viewed by an observer. The luminance of the source or sink in the direction of the observer is the intensity in that direction divided by the projected area.

The luminance exitance is the density of luminous flux leaving a surface of a solar energy absorber. The reflectance is the ratio of the luminous flux reflected from a surface to the luminous flux incident on that surface. The transmittance is the ratio of the luminous flux transmitted through a surface to that incident on the same surface.

Quantity of Sources: Quantity of sources is luminous energy and is related to luminous flux, which is luminous power per unit time.

### 2.2 Radiation sources

The sources of radiation are classified according to the type of wave of interference (Dehra, 2007c, Dehra 2006):

Light: The light is a visual sensation evaluated by an eye with seeing of a radiant energy in the wavelength band of electromagnetic radiation from approximately between 380 to 765 nm (nm = nanometer = $(10^9 + 1)^{-1}$ meter). The units of light are based on the physiological response of a standard (average) eye. The human eye does not have the same sensitivity to all wavelengths or colors. The solar energy spectrum in the visible region contributes in adding daylight as a visual sensation to the human body.

Sound: The sound is a hearing sensation evaluated by ear due to fluid pressure energy in the frequency band approximately between 20 Hz and 20,000 Hz. The units of sound are based on the physiological response of the standard (average) ear. The human ear does not have the same sensitivity to the whole frequency band.

Heat: The heat is a sensation of temperature evaluated by a radiant energy in the wavelength band of electromagnetic radiation from approximately between 0.1 μm to 100 μm (μm = micrometer = $(10^6 + 1)^{-1}$ meter). The units of heat are function of sensation of temperature. The sensation of temperature is a measure of hotness and coldness. Thermal comfort is an evaluation of comfort zone of temperature on the basis of physiological response of a standard (average) human body. The solar energy spectrum in the ultra violet radiation region contributes to sensation of discomfort of the human body.

Electricity: The electricity is a sensation of shock evaluated by skin of an observer due to an electromagnetic energy stored in a conductor short-circuited by a human body either due to pass of direct current or an alternating current.

Fluid: The fluid is a combined sensation of ventilation and breathing evaluated by the amount of fluid passed either externally or internally through a standard (average) human body.

Fire: The fire is a sensation of burning caused due to combined exposure of skin to radiation energy and fluid acting on a standard (average) human body.

### 2.3 Diffraction of radiation sources

The diffraction of radiation sources is termed as interference of noise. The interference of radiation sources are based on areas of energy stored in a wave due to interference, speed of wave and difference of power between two intensities of wave (Dehra, 2008b).

Noise of Sol: The noise of sol (S) is noise occurring due to difference of intensities of power between two solar systems. The amplitude of a solar energy wave is defined as the power storage per unit area per unit time. The solar power is stored in a packet of solar energy wave of unit cross sectional area and of length s, the speed of light.

Noise of Therm: The noise of therm is noise due to difference of intensities of power between two heat power systems. The amplitude of a heat wave is defined as the power storage per unit area per unit time. The heat power is stored in a packet of heat wave of unit cross sectional area and of length s, the speed of light.

Noise of Photons: The noise of photons is noise due to difference of intensities of power between two lighting systems. The amplitude of a light beam is defined as the power storage per unit area per unit time. The light power is stored in a packet of light beam of unit cross sectional area and of length s, the speed of light.

Noise of Electrons: The noise of electrons is noise due to difference of intensities of power between two electrical power systems. The amplitude of an electricity wave is defined as the

power storage per unit area per unit time. The electrical power is stored in a packet of an electricity wave of unit cross sectional area and of length s, the speed of light.
Noise of Scattering: The noise of scattering is noise due to difference of intensities of power between two fluid power systems. The amplitude of a fluid wave is defined as the power storage per unit area per unit time. The fluid power is stored in a packet of fluid energy wave of unit cross sectional area and of length s, the speed of fluid.
Noise of Scattering and Lightning: The noise of scattering and lightning is a noise due to difference of intensities of power between two fire power systems. The amplitude of a flash of fire is defined as the power storage per unit area per unit time. The fire power of light is stored in a packet of flash of fire of unit cross sectional area and of length s, the speed of light. The fire power of fluid is stored in a packet of flash of fire of unit cross sectional area and of length s, the speed of fluid.
Noise of Elasticity: The noise of elasticity is a noise due to difference of intensities of power between two sound power systems. The amplitude of a sound wave is defined as the power storage per unit area per unit time. The sound power is stored in a packet of sound energy wave of unit cross sectional area and of length s, the speed of sound.

### 2.4 Measurement of interference of radiation sources

The measurement equations for measuring interference of radiation sources are presented herewith (Dehra, 2008b).
Noise of Sol: The solar power intensity I is the product of total power storage capacity for a packet of solar energy wave and the speed of light. The logarithm of two solar power intensities, $I_1$ and $I_2$, gives power difference for two solar power intensities. It is mathematically expressed as:

$$\text{Sol} = \log \left(I_1\right) \left(I_2\right)^{-1} \tag{4}$$

Where, Sol is a dimensionless logarithmic unit for noise of sol. The decisol (dS) is more convenient for solar power systems. Since a decisol (dS) is 1/11th unit of a Sol, it is mathematically expressed by the equation:

$$\text{dS} = 11 \log \left(I_1\right) \left(I_2\right)^{-1} \tag{5}$$

Noise of Therm: The heat power intensity I is the product of total power storage capacity for a packet of heat energy wave and the speed of light. The packet of solar energy wave and heat energy wave, have same energy areas, therefore their units of noise are same as Sol.
Noise of Photons: The light power intensity I is the product of total power storage capacity for a packet of light energy wave and the speed of light. The packet of solar energy wave and light energy wave, have same energy areas, therefore their units of noise are same as Sol.
Noise of Electrons: The electrical power intensity I is the product of total electrical storage capacity for a packet of electricity wave and the speed of light. The packet of solar energy wave and an electricity wave, have same energy areas, therefore their units of noise are same as Sol.
Noise of Scattering: The fluid power intensity I is the product of total power storage capacity for a packet of fluid energy wave and the speed of fluid. The logarithm of two fluid

power intensities, $I_1$ and $I_2$, gives power difference for two fluid power intensities. It is mathematically expressed as:

$$\text{Sip} = \log \left(I_1\right) \left(I_2\right)^{-1} \tag{6}$$

Where, Sip is a dimensionless logarithmic unit for noise of scattering. The decisip (dS) is more convenient for fluid power systems. Since a decisip (dS) is 1/11th unit of a Sip, it is mathematically expressed by the equation:

$$\text{dS} = 11 \log \left(I_1\right) \left(I_2\right)^{-1} \tag{7}$$

The water is a standard fluid used with a specific gravity of 1.0 for determining the energy area for a fluid wave.

Noise of Scattering and Lightning: The intensity, I, of flash of fire with power of light, is the product of total power storage capacity for a packet of fire wave and the speed of light. The intensity, I, of flash of fire with power of fluid, is the product of total power storage capacity for a packet of fire wave and speed of fluid.

The combined effect of scattering and lightning for a noise due to flash of fire is to determined by superimposition principle.

- The packet of solar energy wave and a flash of fire with power of light, have same energy areas, therefore their units of noise are same as Sol. The flash of fire with power of light may also include power of therm.
- The packet of fluid energy wave and a flash of fire with power of fluid, have same energy areas, therefore their units of noise are same as Sip. A multiplication factor of a specific gravity of fluid is used in determining the areas of energy for the case of fluids other than water.

Noise of Elasticity: The sound power intensity I is the product of total power storage capacity for a packet of sound energy wave and the speed of sound.

The logarithm of two sound power intensities, $I_1$ and $I_2$, gives power difference for two sound power intensities. It is mathematically expressed as:

$$\text{Bel} = \log \left(I_1\right) \left(I_2\right)^{-1} \tag{8}$$

Where, Bel is a dimensionless logarithmic unit for noise of elasticity. The decibel (dB) is more convenient for sound power systems. Since a decibel (dB) is 1/11th unit of a Bel, it is mathematically expressed by the equation:

$$\text{dB} = 11 \log \left(I_1\right) \left(I_2\right)^{-1} \tag{9}$$

## 3. The roughness factors

The utilisation of solar energy is based on selective design of solar energy absorbers. The minimal flow resistance is required for critical design so that there is maximum absorptance of solar energy at the optimum roughness of the surface. The solar collectors and ducts used

for heating, ventilation and air conditioning (HVAC) and hot water have fluid resistance due to friction losses and dynamic losses. For fluid flow in conduits, the friction loss is calculated by Darcy equation:

$$\Delta p_f = \frac{f\,L}{D_h}\,\frac{\rho\,V^2}{2} \tag{10}$$

Where, $\Delta p_f$ is friction loss in terms of total pressure (Pa); f is friction factor, dimensionless; L is duct length, m; $D_h$ is equivalent hydraulic diameter, m; V is velocity of fluid, m/s and ρ is density of fluid, kg/m³. For a region of laminar flow (Reynolds number less than 2000), the friction factor is a function of Reynolds number only.
For turbulent fluid flow, the friction factor depends on Reynolds number, duct surface roughness, and internal protuberances such as joints. The region of transitional roughness zone lies in between the bounding limits of hydraulically smooth behaviour and fully rough behaviour and for this region of transitional roughness, the friction factor depends on both roughness and Reynolds number. For this transitionally rough , turbulent zone the friction factor, f is calculated by Colebrook's equation. Colebrook's transition curve merges asymptotically into the curves representing laminar and completely turbulent flow.

$$\frac{1}{\sqrt{f}} = -2\log\left(\frac{\varepsilon}{3.7\,D_h} + \frac{2.51}{Re\sqrt{f}}\right) \tag{11}$$

Where, ε is absolute roughness factor (in mm) for material of a solar energy absorber and Re is Reynolds number. Reynolds number is calculated by using the following equation:

$$Re = \frac{D_h \cdot V}{\upsilon} \tag{12}$$

Where, υ is kinematic viscosity, m²/s. For standard air, Reynolds number is calculated by:

$$Re = 0.0664\,D_h\,V \tag{13}$$

The roughness factors, ε are listed in Table 1.

## 4. Human environmental health

Your body acts as a solar energy absorber, which enable your senses for interpretation of our surrounding environment. Your body when exposed to solar radiation releases heat by radiation and conduction. The amount of heat you loose is a function of the difference in temperature between the surface of your body and the environment. The greater is the difference in temperature, the greater the heat loss would be. The heat would be released from your body, if the surface temperature of your body is higher than that of the environment. If due to excessive solar radiation, the environmental temperature rises above your body temperature, you will gain heat from the environment.
Another important method of loosing heat is through evaporation. After swimming, when you come out of the water, there is evaporation of water from your skin and you feel cool.

| Duct Material | Roughness Category | Absolute Roughness, ε, mm |
|---|---|---|
| Uncoated carbon steel, clean (0.05 mm)<br>PVC plastic pipe (0.01 to 0.05 mm)<br>Aluminium (0.04 to 0.06 mm) | Smooth | 0.03 |
| Galvanized steel, longitudinal seams, 1200 mm joints (0.05 to 0.10 mm)<br>Galvanised steel, continuously rolled, spiral seams, 3000 mm joints (0.06 to 0.12 mm)<br>Galvanised steel, spiral seam with 1, 2 and 3 ribs, 3600 mm joints (0.09 to 0.12 mm) | Medium smooth | 0.09 |
| Galvanised steel, longitudinal seams, 760 mm joints (0.15 mm) | Average | 0.15 |
| Fibrous glass duct, rigid<br>Fibrous glass duct liner, air side with facing material (1.5 mm) | Medium rough | 0.9 |
| Fibrous glass duct liner, air side spray coated (4.5 mm)<br>Flexible duct, metallic (1.2 to 2.1 mm when fully extended)<br>Flexible duct, all types of fabric and wire (1.0 to 4.6 mm when fully extended)<br>Concrete (1.3 to 3 mm) | Rough | 3.0 |

Table 1. Roughness factors for some common duct materials.

The water molecules on your body surface must have minimum amount of energy for evaporation. The faster moving water molecules can overcome the forces holding them in the liquid state and bound off into the air as water vapour molecules. The slower and therefore cooler molecules are left behind. Heat then flows from the warmer surface of your skin to the cooler water molecules. This flow of heat transfers energy to the water, speeding the water molecules up so that more of them escape. This cooling of your skin surface also cools any blood which tends to flow through that part of your body. Sweating is a noticeable way to lose heat by evaporation. During the process of sweating, water continuously evaporates from your skin. There is also a small loss of water from the surface of the lungs when you breathe. The amount of water that evaporates, when you breathe or sweat, depends on the humidity of the air. When the humidity of the surrounding air is high, water evaporates much more slowly and therefore contributes less to the cooling process.

### 4.1 Effects of intense heat

Your presence in a room with high air temperature, radiation and conduction do not work in your favour for loss of body heat. Instead of loosing heat from the surface of your body to the surroundings, you gain heat. You can survive, but now sweating is the only mechanism you have for losing heat. The normal response of your body is intense heat strains of the circulatory system. This follows because the hypothalamus responds to the increased heat by causing the blood vessels in your skin to expand. This leads to a decreased resistance to blood flow and your blood pressure tends to fall. Reflexes which prevent large changes in

blood pressure then begin to operate and the decreased resistance to blood flow is compensated for by the heart working harder. The expanded blood vessels make it possible for large amounts of blood to pool in the vessels of your skin at the expense of other organs. If as a result, the blood supply to your brain becomes sufficiently low, you will faint.
Sweating may also create a circulatory problem because of the salt and water loss. Excessive fluid loss causes a decreased plasma volume. This may slow down the output of blood from the heart, which could lead to decreased blood flow to the skin, which in turn could reduce sweating. If this happened, your main avenue for heat loss would be closed. In that event heat production would continue and your body temperature would rise until your whole system is collapsed. The body's ability to control heat loss is limited. When heat can not be lost rapidly enough to prevent a rise in body temperature, a vicious circle may occur. When heat regulation fails, the positive feedback loop (Heat production – metabolism – temperature control) goes into operation; if unchecked it ends in heat stroke and death.
In order to support the case of heat loss from your body, a mathematical analysis of a solar thermosyphon is illustrated. This is followed by presenting some experiments conducted on photovoltaic duct wall. Your body follows the thermosyphon principle for loss of heat. The example of photovoltaic duct wall illustrates the production of heat, metabolism for heat production rate and temperature control in your body.

## 5. Mathematical analysis of a solar thermosyphon

The mathematical analysis has been performed for steady heat conduction and heat transport analysis of a solar thermosyphon (Dehra, 2007d). The analysis has been conducted on system geometry of a solar thermosyphon with discretisation of its total covered volume into surface and air nodes located by formulation of the control volumes. As illustrated in Fig. 1, thermosyphon is placed along the y-axis with y = 0 near the bottom end of the system boundary and y = H near the top end of the system boundary. The solar thermosyphon is rectangular in cross-section with width W in z-direction and air-gap length, L in x-direction. The thermal conductivities of outer wall and inner wall are assumed to be constant along their dimensions-L, W and H. The inner wall is well-insulated with thermal conductance $u_i$. The outer wall is of good thermal conductance ($u_o$) for conducting heat flux of solar irradiation. The heat transfer between building space and well-insulated inner wall is nil. The heat transfer between side walls of length L, and height H and surrounding zone is nil. The air passage of thermosyphon system is connected with the building space through a damper operating system. The physical domain of the thermosyphon is analysed as a parallel-plate channel. The climatic and thermal design data has been kept constant in the steady heat flow analysis of a solar thermosyphon. Single climatic variable of ambient air temperature, solar irradiation and building zone air temperatures are known constants in the analysis. The unique characteristics of the improved numerical solution method are: i) inclusion of conduction heat flow along height of outer and inner walls of thermosyphon; and (ii) inclusion of radiation exchange calculations using radiosity-irradiation method by assuming enclosure between outer and inner walls of thermosyphon. The resultant affect of conjugate heat exchange and heat transport on temperature distribution in thermosyphon has improved the accuracy of the numerical method over analytical method.
The key assumptions and initial conditions used in mathematical analysis are: (i) outer wall is thin, light weight and good conductor of heat; (ii) the net solar heat flux, $q_o$ on the outer wall is quasi steady-state and distributed uniformly over the surface; (iii) inner wall is light

weight and good insulator for heat; (iv) temperature variation only along y-ordinate, being taken as lumped in x and z-coordinates; (v) heat conduction (diffusion) equation term with negligible value for air is not included in the energy balance; (vi) heat transfer between the side walls/inner wall of the thermosyphon and the surrounding environment is negligible; (vii) temperatures of ambient air ($T_a$) and single building air zone ($T_s$) are specified. As illustrated in Fig. 2, nodal or lattice points are created in the rectangular mesh at which temperatures are to be approximated. The nodal points are created after dividing the thermosyphon system into control volumes. The distance between control volume nodes on x-y plane is $\Delta x_o=(t_o+L)/2$, $\Delta x_i=(t_i+L)/2$ for outer wall and inner wall in x-ordinate and $\Delta y$ in y-ordinate. The control volumes are lumped sub system, in which temperature represented at the node represent the average temperature of the volume. The computational grid is developed by drawing five vertical construction lines at distance x = 0, $t_o$, ($t_o$ + L/2), ($t_o$ + L), and ($t_o$ + $t_i$ + L) apart and ten horizontal construction lines at $\Delta y$ distance apart starting from y=$\Delta y$/2. Nodes are located at all the intersections of the construction lines. The control volumes are formed by drawing horizontal and vertical lines that exist midway between adjoining construction lines. The control volumes formulated are solid up to width of the outer or the inner wall and continued with made up of air of width (L/2). Surface nodes are located midway and air nodes are located on the edges of the control volume. Air-nodes are common to the two adjoining solid-air and air-solid control volumes.

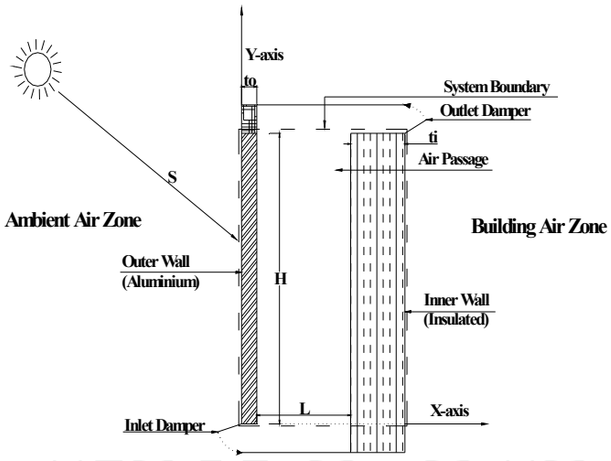


Fig. 1. Schematic of a solar thermosyphon integrated to building air zone

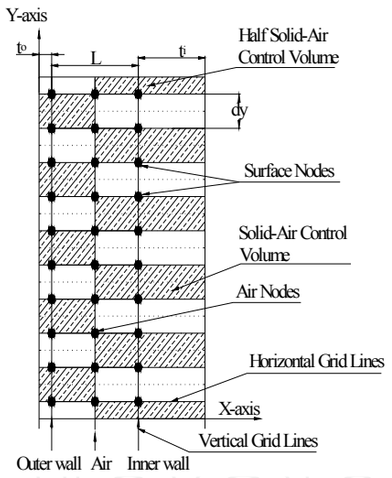


Fig. 2. Discretisation of a solar thermosyphon into control volumes, cell faces and nodes

### 5.1 Initial Boundary Value Problem (IBVP)

Initial boundary value problem is formulated as per initial conditions and boundary conditions. For the outer wall with uniform heat flux, heat conduction equation is written with boundary conditions as (Dehra 2007d):

$$\frac{\partial^2}{\partial x^2}T_o + \frac{\partial^2}{\partial y^2}T_o + \frac{q_o}{k_o} = 0 \qquad \text{in} \quad 0 < x < t_o \qquad 0 < y < H \tag{14}$$

$$-\left(\frac{\partial}{\partial x}T_o\right) = \frac{\alpha\, S - h_a\left(T_o - T_a\right)}{k_o} \qquad \text{at} \quad x = 0 \tag{15}$$

$$\frac{\partial}{\partial x}T_o = \frac{h_o\left(T_o - T_f\right) + hr\left(T_o - T_i\right)}{k_o} \qquad \text{at} \quad x = t_o \tag{16}$$

For the inner wall with insulation, heat conduction equation with boundary conditions is:

$$\frac{\partial^2}{\partial x^2}T_i + \frac{\partial^2}{\partial y^2}T_i = 0 \qquad \text{in} \quad L + t_o < x < L + t_o + t_i \qquad 0 < y < H \tag{17}$$

$$\frac{\partial}{\partial x}T_i = \frac{h_s\left(T_i - T_s\right)}{k_i} = 0 \qquad \text{at} \quad x = L + t_o + t_i \tag{18}$$

$$-\left(\frac{\partial}{\partial x}T_i\right) = \frac{h_i\left(T_i - T_f\right) + hr\left(T_i - T_o\right)}{k_i} \qquad \text{at} \quad x = L + t_o \tag{19}$$

Heat transport equation for air with its boundary value as:

$$\theta(y)\left[\frac{\partial}{\partial y}T_f(y)\right] + T_f(y) - \left[\frac{T_o(y) + T_i(y)}{2}\right] = 0 \qquad \text{in} \quad 0 < y < H \tag{20}$$

$$T_f(y) = T_f(k) \qquad \text{at} \quad y = \left(k + \frac{1}{2}\right)\cdot\frac{H}{n} \qquad k = 0..(n-1) \tag{21}$$

In Eq. 21, *k* varies from 0 to (n-1), where n is number of nodes in y-ordinate. θ(y) =θ is constant within the control volume at steady flow conditions, defined by following expression:

$$\theta = \frac{v\,\rho\,L\,c_p}{h_c\,W} \tag{22}$$

### 5.2 Semi-analytical method

The partial differential equations are solved by applying initial conditions and lumped parameter assumption to get the analytical solution. The temperatures of outer wall, inner wall and air are obtained as:

$$T_o = \frac{h_a\,T_a + h_o\,T_f + hr\,T_i + \alpha\,S}{h_o + hr + h_a} \qquad \text{for} \quad \left(\frac{\partial}{\partial x}T_o\right)_{x=0} = \left(\frac{\partial}{\partial x}T_o\right)_{x=t_o} \tag{23}$$

$$T_i = \frac{h_s\cdot T_s + h_i\cdot T_f + hr\cdot T_o}{h_i + hr + h_s} \qquad \text{for} \quad \left(\frac{\partial}{\partial x}T_i\right)_{x=t_o+L} = \left(\frac{\partial}{\partial x}T_i\right)_{x=t_o+L+t_i} \tag{24}$$

$$T_f = \frac{T_o + T_i}{2} + \left[ T_f \cdot (k) - \frac{T_o + T_i}{2} \right] \cdot e^{-2 \cdot \frac{\Delta y}{\theta}} \tag{25}$$

Where, $\Delta y = H/n$ is discretisation height of the control volume. Equation (6) is applicable with in the control volume and it predicts particular solution for each $\Delta y$ from the values of $T_f(k)$ at previous air node. The exponential solution of Equation (6) is semi-analytical in nature because of its applicability for the nodes with in the physical domain of Fig. 1(b).

The numerical solutions are obtained by creation of additional heat exchange paths in the computational grid. The additional heat exchange paths are created by incorporating conduction heat flow along height of walls of thermosyphon and integrated radiation heat exchange between composite surface nodes of outer and inner walls of thermosyphon (Dehra, 2004). The numerical analysis involves (i) construction of nodal networks; (ii) energy balance on the surface nodes located at solid-air edges of the walls; (iii) energy balance on control volume for air passage; and (iv) computer solution of system of algebraic equations. The energy balance equations for the N nodes involves formulation of $(U_{N,N})$-matrix with conductance terms and heat source elements $(Q_{1,N})$. Conductance terms describe entropy flux over the discretised area (in W/K units) at the node. Inverse of U-matrix is multiplied with heat source matrix to give temperature solution of the thermal network. In writing nodal equations in matrix form, sign notation is adopted for automatic formulation of U-matrix with unknown temperatures and heat source elements. Sum of all incoming heat source elements and U-matrix conductance terms multiplied with temperature difference with respect to the unknown temperatures at other nodes are equal to zero. The energy balance is written in equation form for any general node (m,n) as per sign notation:

$$\sum_{n=1}^{N} \left( U_{m,n} \times \Delta T_{m,n} \right) + \sum_{n=1}^{N} Q_{m,n} = 0 \tag{26}$$

Where $U_{m,n}$ is the conductance at node (m,n), $\Delta T_{m,n}$ is the difference between unknown temperature at the node (m,n) and unknown temperature at surrounding heat exchange node. $Q_N$ is heat source term at the node (m,n). The detail of numerical method is provided in (Dehra, 2004) and is omitted here by presenting its numerical solution procedure (Dehra, 2008a):

Step 1. Thermal properties are used to initialise the numerical solution. The conductance values are calculated as per constitutive relations for conduction, convection, radiation and heat transport.

Step 2. The corrected iterated value of the mass flow rate as depicted in Table 2 is obtained from the numerical solution and is used for obtaining thermal capacity conductance values.

Step 3. The heat transfer coefficients are calculated using temperatures obtained from the analytical solution. The values of convective heat transfer coefficients obtained from semi-analytical solution are also used in obtaining the numerical solution.

Step 4. The effect of integrated radiation heat exchange between surface nodes of outer and inner wall is considered with radiosity-irradiation method assuming enclosure analysis (Dehra, 2004). The radiation heat exchange factors are calculated for each node using script factor matrix of size (20 X 20). Using radiation heat exchange factors radiation conductance values are calculated, which also form matrix (20 X 20).

Step 5. Once conjugate heat exchange conductance values for 30 nodes are calculated, U-matrix of size (30 X 30) is formulated. The U-matrix is formulated by obtaining off-diagonal and diagonal entries as per constitutive relations and sign convention. The inverse of U-matrix (30 X 30) is multiplied with heat source element matrix (1 X 30), to obtain temperatures at 30 nodes (30 X 1) as per Equation (26).

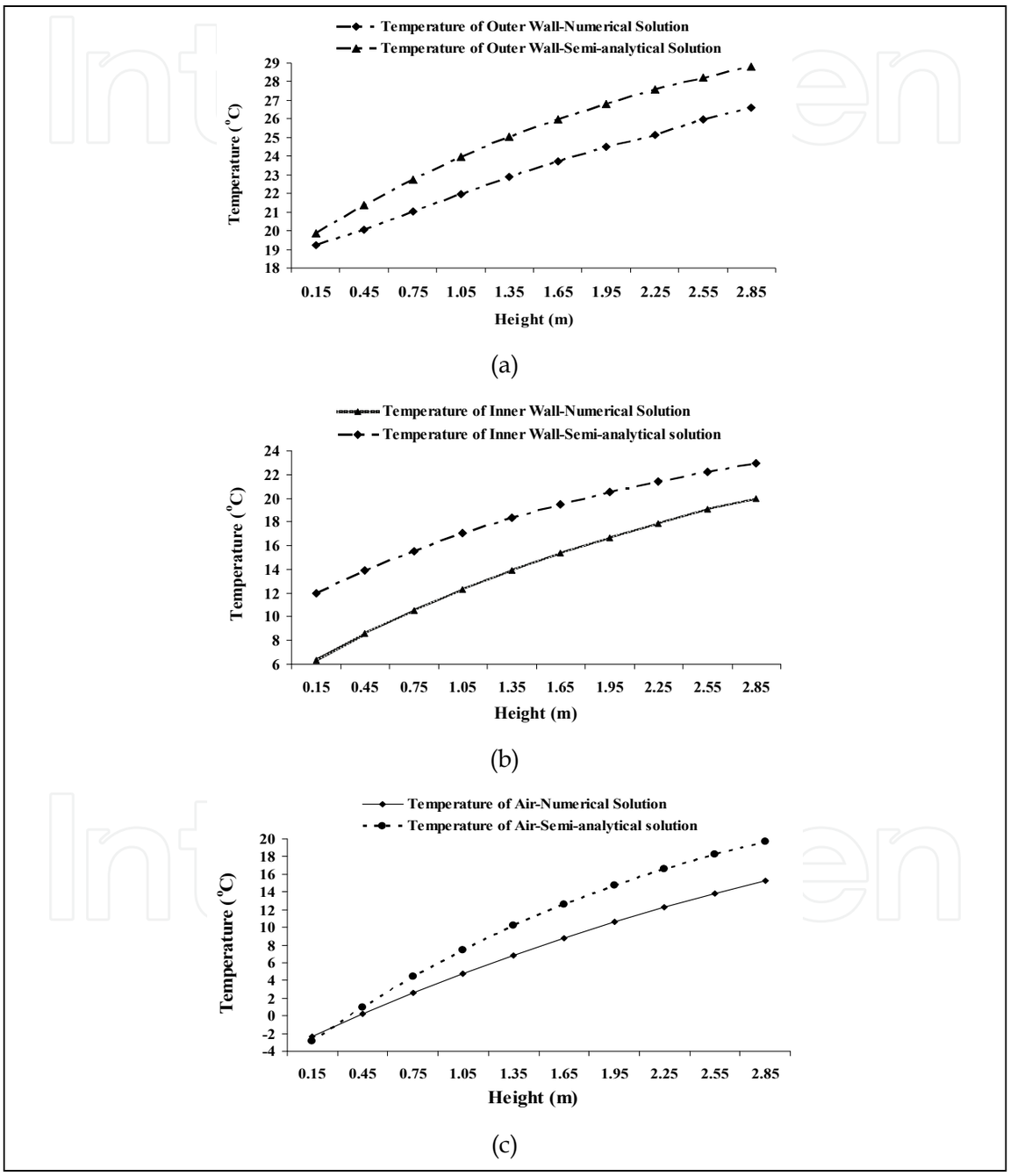


Fig. 3. Comparison of temperature profiles from semi-analytical and numerical solutions with height of solar thermosyphon for (a) outer wall; (b) inner wall; and (c) air

Figure 3 has compared the results obtained from traditional analytial model and numerical model. A matrix solution procedure is adopted for solving energy balance nodal equations at surface and air nodes. The improved numerical method has considered the effect of thermal storage by incorporating conduction heat flow factors in y-direction for outer and inner walls of thermosyphon. The heat conduction and radiation heat exchange between surface nodes has improved the accuracy of a traditional analytical solution for predicting buoyancy-induced mass flow rate through a solar thermosyphon. The conduction and convection conductance terms are based on discretisation height $\Delta y$, thermal capacity conductance ($mc_p$) is based on air-gap length $\Delta x$, whilst integrated radiation conductance terms are based on both height $\Delta y$ and width $\Delta x$ of the grid. The constitutive relations for obtaining conductance terms for conductance (U's) matrix are calculated over discretised control areas in y-z plane for conduction heat flow, radiation and convection heat exchange. Whilst, heat transport conductance terms are calculated from mass flow rate crossing the control volume in x-z plane assuming no leakage or infiltration sources in the thermosyphon.

## 6. Photovoltaic duct wall

In an effort to enhance overall efficiency of PV module power generation system, a novel solar energy utilization technique for co-generation of electric and thermal power is analyzed with a photovoltaic duct wall system. A full scale experimental facility for a photovoltaic duct wall was installed at Concordia University, Montréal, Concordia (Dehra, 2004). The photovoltaic duct wall was comprised of a pair of glass coated PV modules, ventilated air passage and polystyrene filled plywood board. In this case duct wall with air ventilation acts as cooling channel for PV modules by reducing surface temperature of solar cells in PV modules and slightly increases its efficiency for electric power generation. With air as fluid medium, assessment of the potential use of photovoltaic duct wall to be used as a source of co-generation of electric and thermal power can be performed by thermal analysis of material properties of photovoltaic duct wall system (PV module, air and plywood board). The thermal analysis of a photovoltaic duct wall has been performed through experimental and numerical investigations. The measurement data collected from the experimental setup was for solar intensities, currents, voltages, air velocities and temperatures of air and composite surfaces. The measured temperatures were obtained as a function of height of photovoltaic duct wall. The heat transfer rate from a photovoltaic duct wall is a measure of heat storage and thermal storage capacities of its various components. The steady state heat transfer rate has been predicted by performing two dimensional energy and mass balances on discretised section of photovoltaic duct wall, to get solutions of one dimensional heat conduction and heat transport equations. The assumptions of steady state heat transfer and lumped heat capacity are validated by comparing heat losses along all major dimensions. The non-consideration of transient analysis has been justified by comparing thermal losses along all major dimensions.

### 6.1 Experimental setup

The photovoltaic duct wall was installed on south facing façade of prefabricated outdoor room. The outdoor room was setup at Concordia University, Montréal, Québec, Concordia for conducting practical investigations (Dehra 2004, Dehra 2007a, Dehra 2009). The photovoltaic duct wall was vertically inclined at 10° East of South on the horizontal plane. The test section of photovoltaic duct wall was assembled in components with two commercially available PV modules, air passage with air-gap width of 90 mm, plywood board

filled with polystyrene as insulation panel, side walls made up of Plexiglas and all parts connected with wooden frames. The photovoltaic duct wall section was constructed with two glass coated PV modules each of dimensions: (989 mm X 453 mm). The PV modules were having glass coating of 3 mm attached on their exterior and interior sides. The plywood board was assembled with 7 mm thick plywood board enclosure filled with 26 mm polystyrene. The overall thickness of plywood board with polystyrene was 40 mm. The exterior dampers were made of wood covered with an aluminium sheet. The heating, ventilating and air-conditioning (HVAC) requirements were met in the outdoor room by a baseboard heater, an induced-draft type exhaust fan and a split window air conditioner (Dehra, 2004). The heating was supplemented by conditioning from the fresh air entering from the inlet damper through photovoltaic duct wall. However, during the mild season of autumn for the duration of conducting experimental runs, neither baseboard heater was used nor air-conditioning unit was used for auxiliary heating or cooling inside the pre-fabricated outdoor room.

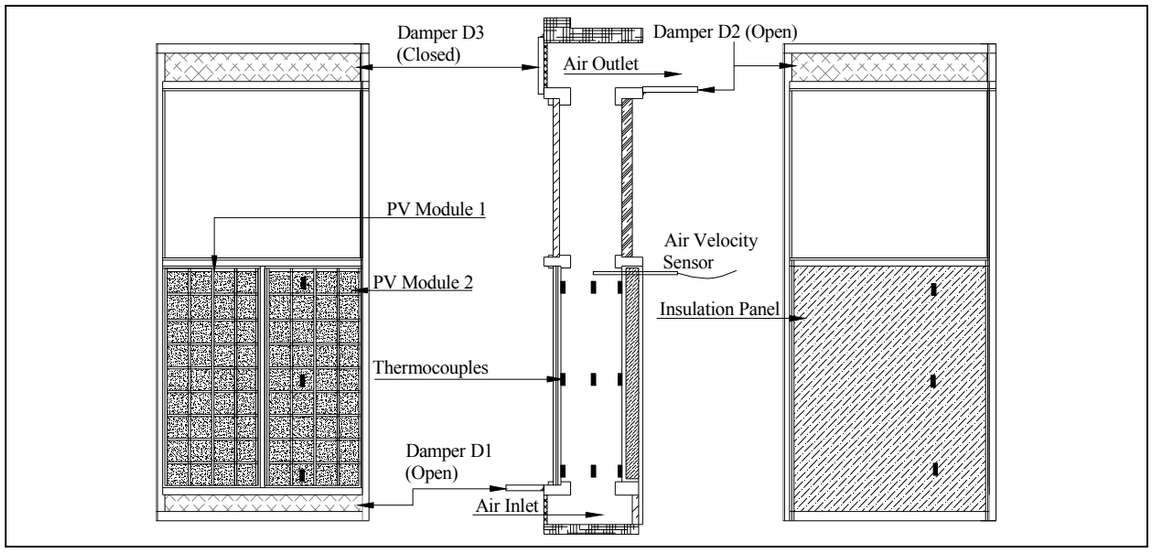


Fig. 4. Schematic of the Experimental Setup

The pair of PV modules used for conducting experimental investigations was connected in series for generation of electric power with a rheostat of maximum varying resistance up to 50 Ω. T-type thermocouples were used for obtaining thermal measurements from the test section of photovoltaic module. As is illustrated in Fig. 4, three thermocouple sensors were placed at the top, middle and bottom locations in the PV module, air-passage and insulation panel of plywood board filled with polystyrene were used to measure local temperatures. Two thermocouples were used to measure the inside test room air temperature and ambient air temperature. The hybrid air ventilation created for the PV module test section was by natural wind, or through buoyancy effect in the absence of wind (Dehra, 2004). The fan pressure was used to achieve higher air velocities by operation of the exhaust fan fixed on opposite wall with respect to wall of the test section (Dehra, 2004). The slight negative pressure was induced for drawing low air velocities in absence of wind-induced pressure from the inlet damper into the test section through the test room (Dehra, 2004). Air velocity sensor was placed perpendicular to the walls of the PV module test section to record axial air velocities near its outlet. The thermocouple outputs, currents, voltages, solar irradiation and air velocity signals were connected to a data logger and a computer for data storage. The measurements collected

from the sensors were recorded as a function of air velocities or mass flow rate from the test section with use of fan pressure. The experimental data from the data acquisition system was collected and stored every two minutes in the computer (Dehra, 2004).

### 6.2 Temperature plots

The measurements collected from the sensors were recorded as a function of air velocities through the PV module test section (Dehra, 2004): (i) Hybrid ventilation without use of fan pressure; and (ii) Hybrid ventilation with use of fan pressure. The temperature measurements were obtained from the PV module test section as a function of air velocities. The temperatures were obtained for glass coated PV module, air passage and insulating panel in the wooden frame. The set of sample measurements obtained from outdoor experiments is presented in Table 2. The temperature plots for PV module, insulating panel and air for different hybrid ventilation conditions are illustrated in Figs. 5 and 6. The temperature plots are obtained against the height of PV module test section for the data provided in Tables 2 to 4. The variation of mean temperatures of PV module, insulating panel and air with approximately steady solar noon irradiation with varying mass flow rates for the case of fan-induced hybrid ventilation and buoyancy-induced hybrid ventilation are plotted in Figs. 7 to 9.

| Run No. | S ($W\ m^{-2}$) | $E_p$ (W) | $T_o$ (° C) | $T_s$ (° C) | V ($m\ s^{-1}$) |
|---|---|---|---|---|---|
| Fan-induced hybrid ventilation | | | | | |
| 1 | 716.1 | 30.7 | 15.2 | 22.4 | 0.68 |
| 2 | 716.1 | 30.7 | 13.4 | 22.4 | 0.53 |
| Buoyancy-induced hybrid ventilation | | | | | |
| 3 | 697.5 | 28.9 | 13.2 | 25.1 | 0.13 |
| 4 | 697.5 | 28.8 | 13.3 | 24.9 | 0.17 |

| Run No. | $T_p$(b) (° C) | $T_p$(m) (° C) | $T_p$(t) (° C) | $T_b$(b) (° C) | $T_b$(m) (° C) | $T_b$(t) (° C) | $T_a$(b) (° C) | $T_a$(m) (° C) | $T_a$(t) (° C) |
|---|---|---|---|---|---|---|---|---|---|
| Fan-induced hybrid ventilation | | | | | | | | | |
| 1 | 35.4 | 33.8 | 36.8 | 20.6 | 24.7 | 29.1 | 18.8 | 21.7 | 19.4 |
| 2 | 35.9 | 34.6 | 37.9 | 20.9 | 25.0 | 29.5 | 19.3 | 22.5 | 19.9 |
| Buoyancy-induced hybrid ventilation | | | | | | | | | |
| 3 | 40.8 | 44.9 | 46.8 | 27.9 | 34.8 | 38.0 | 21.3 | 29.5 | 29.8 |
| 4 | 39.9 | 45.0 | 46.8 | 28.4 | 35.0 | 38.3 | 21.7 | 28.3 | 29.8 |

| Distance as per locations shown in Fig. 4 | $T_p$(b) (° C) | $T_p$(m) (° C) | $T_p$(t) (° C) | $T_b$(b) (° C) | $T_b$(m) (° C) |
|---|---|---|---|---|---|
| y (cm) | 15 | 55 | 94 | 15 | 55 |
| z (cm) | 60 | 60 | 60 | 60 | 60 |
| x (mm) | 6.2 | 6.2 | 6.2 | 96.2 | 96.2 |

| Distance as per locations shown in Fig. 4 | $T_b$(t) (° C) | $T_a$(b) (° C) | $T_a$(m) (° C) | $T_a$(t) (° C) | Air velocity sensor |
|---|---|---|---|---|---|
| y (cm) | 94 | 15 | 55 | 94 | 99 |
| z (cm) | 60 | 60 | 60 | 60 | 60 |
| x (mm) | 96.2 | 51.2 | 51.2 | 51.2 | 51.2 |

Note: x is horizontal; y is vertical; z is adjacent 3rd axis of x-y plane

Table 2. Outdoor measurements obtained from the experimental setup

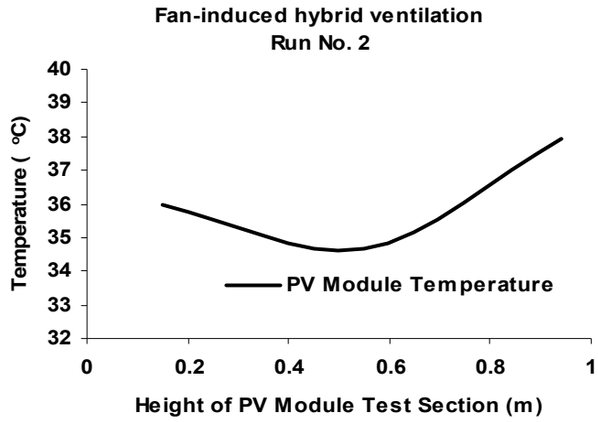


Fig. 5.(a) Temperature plot of PV module for fan-induced hybrid ventilation with height of PV module test section

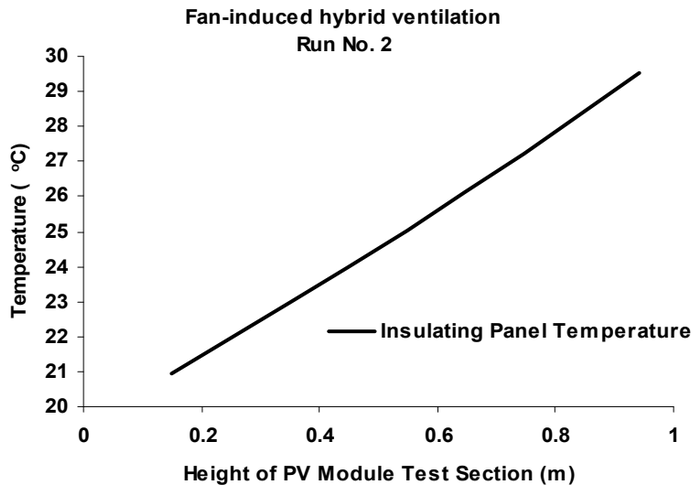


Fig. 5.(b) Temperature plot of insulating panel for fan-induced hybrid ventilation with height of PV module test section

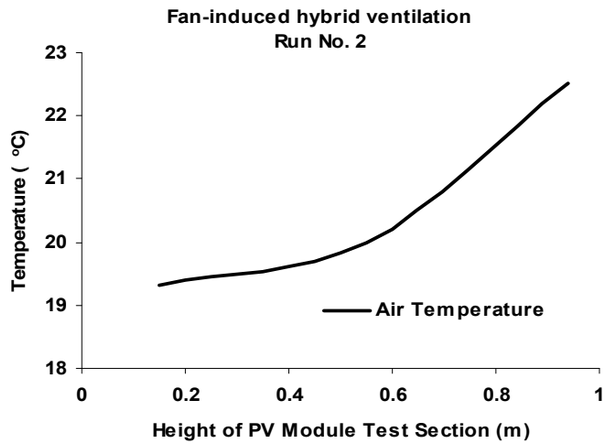


Fig. 5.(c) Temperature plot of air for fan-induced hybrid ventilation with height of PV module test section

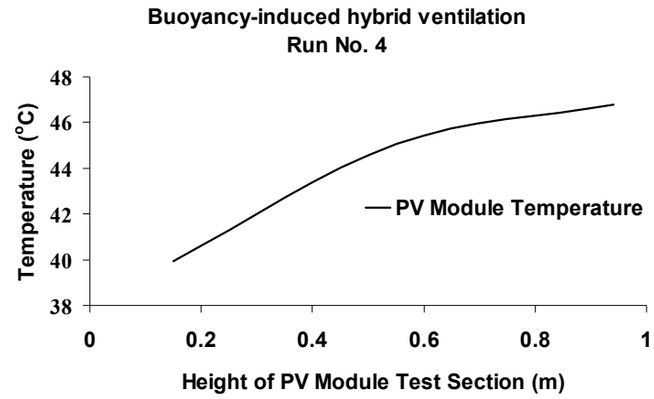


Fig. 6.(a) Temperature plot of PV module for buoyancy-induced hybrid ventilation with height of PV module test section

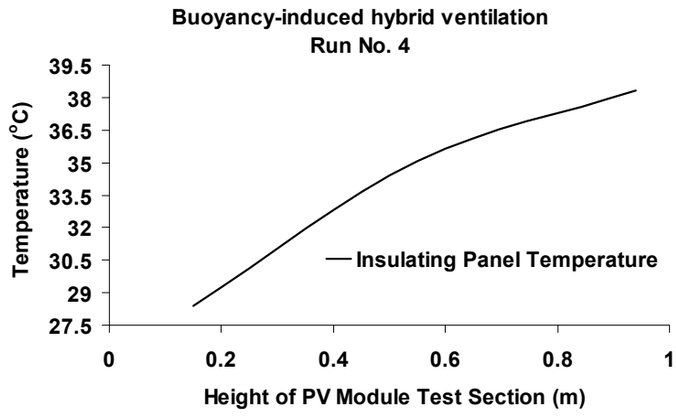


Fig. 6.(b) Temperature plot of insulating panel for buoyancy-induced hybrid ventilation with height of PV module test section

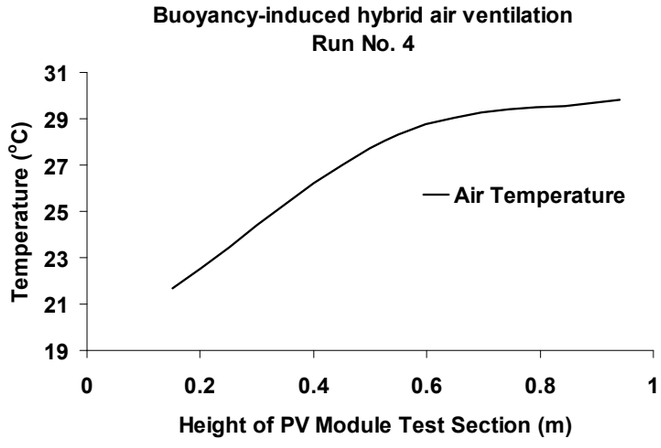


Fig. 6.(c) Temperature plot of air for buoyancy-induced hybrid ventilation with height of PV module test section

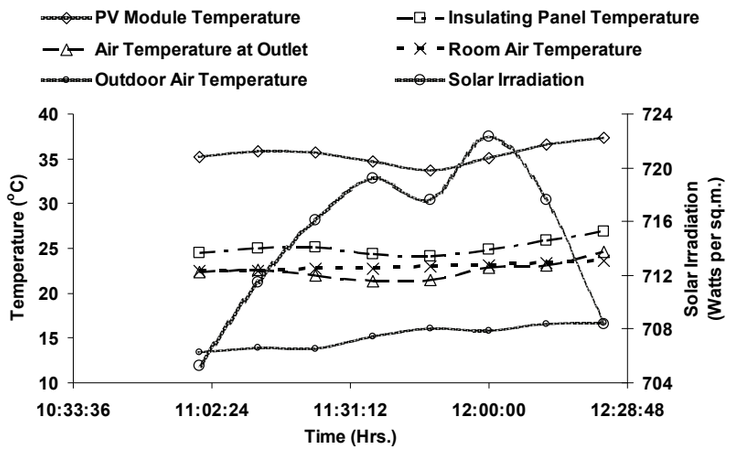


Fig. 7. Variation of mean temperatures of PV module, air and insulating panel with solar irradiation under fan-induced hybrid ventilation

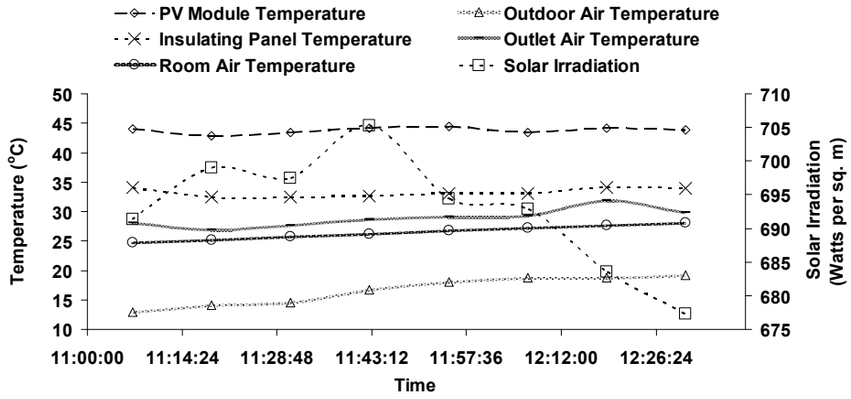


Fig. 8.(a) Variation of mean temperatures of PV module, air and insulating panel with solar irradiation under buoyancy-induced hybrid ventilation

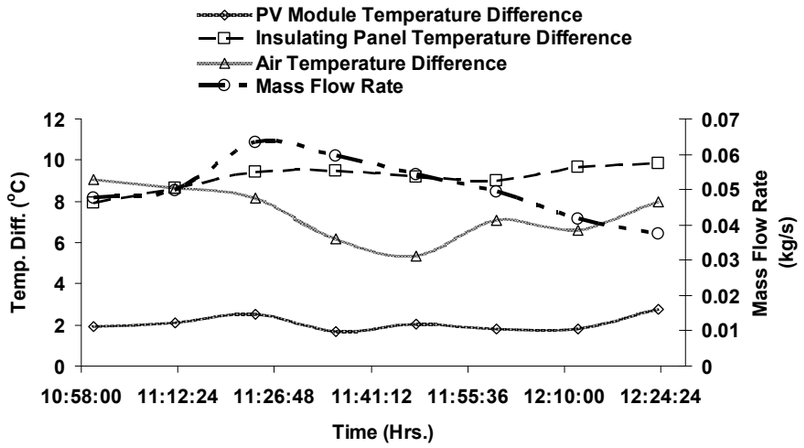


Fig. 8.(b) Temperature difference for PV module, insulating panel and air with height of PV module test section for under fan-induced hybrid ventilation

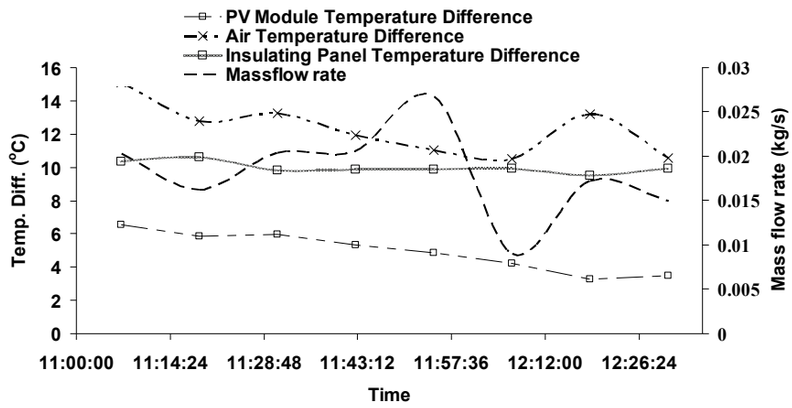


Fig. 9. Temperature difference for PV module, insulating panel and air with height of PV module test section under buoyancy-induced hybrid ventilation

### 6.3 Sensible heat storage capacity

The glass coated PV module test section with wooden frame was composed of non-homogeneous materials having different densities, specific heats and thicknesses (2007 a). The pair of glass coated PV module was having three layers of material viz., a flat sheet of solar cells, with glass face sheets on its exterior and interior sides. The surface temperature of PV module was assumed to be uniformly distributed in the three layers. The heat capacity of the wooden frame and sealing material was having negligible effect on the temperature of PV module, air or insulating panel because wood was used as construction material and moreover the magnitude of the heat capacity of wood framing material was not proportional to the face area of glass coated PV modules. Table 3 has presented sensible heat capacities of glass coating, solar cells, air and polystyrene filled plywood board. For the critical case of buoyancy-induced hybrid ventilation of Run no. 4 in Table 2, it was observed that the difference of temperatures recorded by the top and bottom sensors for PV module, air and insulating panel were 6.9 °C, 8.1 °C and 9.9 °C respectively. The temperature differences were used for obtaining sensible heat storage capacities of various components in y-ordinate. The heat storage capacities calculated were 59.6 kJ, 0.755 kJ and 510.7 kJ for

| Component | $\rho_n$ (kg m$^{-3}$) | $C_n$ (J Kg$^{-1}$ K$^{-1}$) | $d_n$ (m)X10$^{-3}$ | $d_n\rho_nC_n$ (J m$^{-2}$K$^{-1}$) | $H_{pv\text{-}T}$ (J K$^{-1}$) |
|---|---|---|---|---|---|
| Glass coating | 3000 | 500 | 3 | 4500 | 4171.5 |
| PV module | 2330 | 677 | 0.2 | 315.48 | 292.45 |
| Glass coating | 3000 | 500 | 3 | 4500 | 4171.5 |
| Sub-total | - | - | - | - | 8635.5 |
| Air | 1.1174 | 1000 | 90 | 100.56 | 93.22 |
| Plywood | 550 | 1750 | 7 | 6737.5 | 6245.66 |
| Polystyrene | 1050 | 1200 | 26 | 32760 | 30368.5 |
| Plywood | 550 | 1750 | 7 | 6737.5 | 6245.66 |
| Sub-total | - | - | - | - | 42953.0 |
| Total | - | - | - | - | 51588.5 |

Note: Heat capacities were calculated for face area of PV module test section of 0.927 m$^2$.

Table 3. Sensible Heat Storage Capacities

PV module, air and insulating panel respectively. The values of heat capacities predicted were negligible in comparison with the total daily solar irradiation on PV modules on the day of conducting outdoor experiments. The values were estimated by assuming the constant surface properties and ideal still air at the instance of collection of measurements. Similar value of heat storage capacity in x-ordinate was obtained by assuming same proportionate temperature difference along thicknesses in x-ordinate. It was found to be nil in comparison with the value of heat capacity obtained for y-ordinate.

### 6.4 Thermal time constant

Thermal time constant is the time required for the outlet air temperature from the PV module test section to attain 63.2 percent of the total difference in value attained in air temperature following a step change in temperature of outdoor air crossing the inlet opening (Dehra 2007 a). The data was selected observing a step change in the ambient air temperature. The selected data was in steady state before and after the time-interval during the unsteady state response of the outlet air temperature with the step change in ambient air temperature. Thermal time constant under buoyancy-induced hybrid air ventilation was estimated between 8-10 minutes in comparison to 2 minutes estimated under fan-induced hybrid air ventilation. Therefore duration of time interval for obtaining measurements from the data logger was selected for a minimum of two minutes to record any subtle temperature changes. The graphs of outdoor and outlet air temperatures were plotted against the time-interval of measured data for the cases of buoyancy and fan-induced hybrid ventilation are illustrated in Fig. 10(a) and 10(b).

Thermal time constants of the PV module test section were function of ambient air temperatures and air velocities and were therefore approximately calculated under conditions of buoyancy-induced and fan-induced hybrid air ventilation.

### 6.5 Thermal storage capacity

Thermal storage capacities of various components of PV module test section are obtained from their thermal conductivities. Time constant ($T=\rho_d C_{pd} d_d / h_d$) for each component is

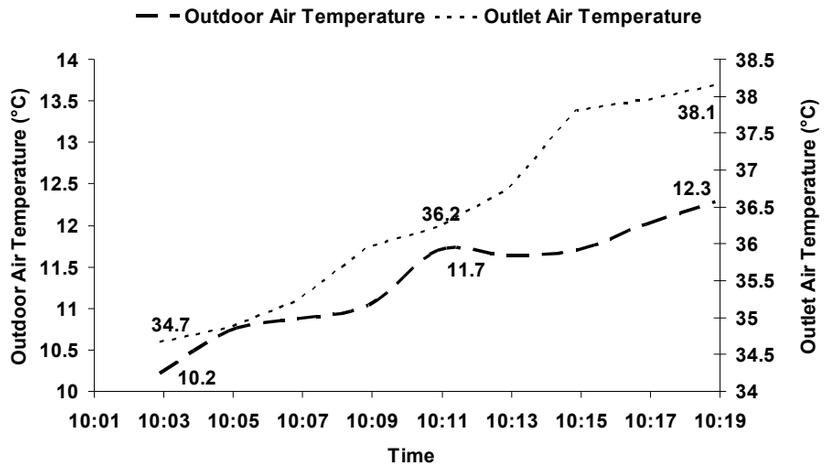


Fig. 10.(a) Changes in outlet air temperature from PV module test section with a step change in outdoor air temperature under buoyancy-induced hybrid ventilation

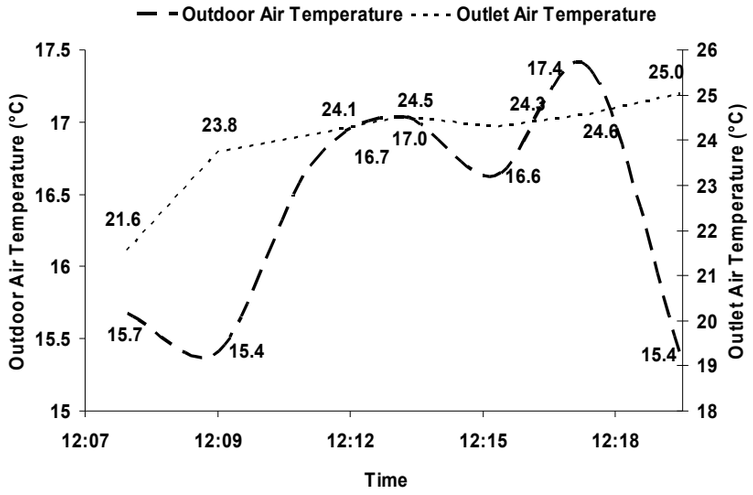


Fig. 10.(b) Changes in outlet air temperature from PV module test section with a step change in outdoor air temperature under fan-induced hybrid ventilation

calculated in units of time from their heat capacities and film coefficients ($Wm^{-2}K^{-1}$). Thermal storage capacity of PV module test section along its height is 15.9 KJ. Thermal storage capacity in x-direction is negligible in comparison with the thermal storage capacity in y-direction. Therefore temperature measurements were also felt necessary along the height of PV module system to consider pattern of heat flow and heat transport. The thermal storage capacities of components of PV module test section are presented in Table 4.

| Component | $k_d$ ($W\ m^{-1}\ K^{-1}$) | $d_n\rho_nC_n$ ($J\ m^{-2}K^{-1}$) | $H_d$ ($Wm^{-2}K^{-1}$) | T (sec) |
|---|---|---|---|---|
| PV module | 0.91 | 9315.48 | 10 | 932 |
| Air | 0.02624 | 100.56 | 10.0 | 10 |
| Plywood | 0.0835 | 6737.5 | 10.0 | 674 |
| Polystyrene | 0.02821 | 32760 | 1.0 | 32760 |
| Plywood | 0.0835 | 6737.5 | 10.0 | 674 |
| Component | $\Delta T_V$ (K) | $\Delta T_H$ (K) | $Q_V$ (KJ) | $Q_H$ (J) |
| PV module | 6.9 | 0.04 | 5.8 | 0.2 |
| Air | 8.1 | 0.75 | 0.0 | 0.0 |
| Plywood | 9.9 | 0.40 | 0.55 | 0.16 |
| Polystyrene | 9.9 | 0.40 | 9.0 | 9.6 |
| Plywood | 9.9 | 0.40 | 0.55 | 0.16 |
| Total | - | - | 15.9 | 10.12 |

Table 4. Thermal Storage Capacities

Notes to the Table 4:

i) Equivalent thermal conductivity of glass coated PV module was calculated to be 0.91 $Wm^{-1}\ K^{-1}$; ii) temperature differences along y-direction i.e. along height of PV module test section (0.993 m) were obtained from Table 2 for Run No. 4 in the case of buoyancy-induced hybrid ventilation.

## 7. Conclusion

Solar energy absorbers use their selective properties for utilisation of solar energy. The theory, analysis and methodology for selective design of solar energy absorbers is presented. The radiation properties, sources of radiation, diffraction and measurement of radiation are presented. The environmental health is discussed by presenting physiology of solar radiation effects on the skin surface and mechanism of entropy generation by solar energy absorbers. The supporting examples of solar thermosyphon and photovoltaic duct wall are presented. The heat and body temperature control for human environmental health is involved by presenting the physiology and metabolism of heat loss from the human body surface. The modeling and experimental results for solar thermosyphon and photovoltaic duct wall are elaborated for illustrating the cases of solar energy absorbers as solar collectors and panels.

## 8. Acknowledgements

The Author (Guru of the Sikhs Dr. Himanshu Dehra) is a Doctor of Public Health Medicine in *Noise Behaviour*. The sovereign King *Guru Shri Shri Shri 1008* Dr. Himanshu Dehra (Emperor of Earth, Wind, Sky and Lord of Moon) is grateful to his thirty two Queens for their worships and allegiances for his everlasting Kingdom and is a capital industrialist of enterprises:

I. Quality Tools & Measurement Systems (QTMS)
II. Quality Guard & Protection Systems (QGPS)
III. Quality Detection & Prevention Systems (QDPS)
IV. Quality Defence & Security Systems (QDSS)
V. Quality Arms & Ammunition Systems (QAAS)
VI. *Gati* Transportation Systems (GTS)
VII. *Mati* Logistics Systems (MLS)
VIII. *Indrani* Corporation (IC)
IX. *Indrani* Securities & Holdings (ISH)
X. *Indrani* Investments & Finances (IIF)
XI. *Indrani* Projects & Controls (IPC)
XII. *Indrani* Laws & Books (ILB)
XIII. *Indrani* Routes & Travels (IRT)
XIV. *Indrani* Herbs & Medicines (IHM)
XV. *Indrani* Designs & Furnishings (IDF)
XVI. *Indrani* Flags & Decorations (IFD)
XVII. *Indrani* Languages & Communications (ILC)
XVIII. *Indrani* Resources & Employees (IRE)
XIX. *Indrani* Commands & Forces (ICF)
XX. *Indrani* Events & Plans (IEP)
XXI. *Indrani* Agencies & Societies (IAS)
XXII. *Indrani* Religions & Worships (IRW)
XXIII. *Indrani* Forests & Timbers (IFT)
XXIV. *Indrani* Productions & Films (IPF)
XXV. *Indrani* Maps & Atlases (IMA)
XXVI. *Indrani* Reports & Presses (IRP)

XXVII. *Indrani* Crops & Animals (ICA)
XXVIII. *Indrani* Palaces & Monuments (IPM)
XXIX. *Indrani* Foods & Dairies (IFD)
XXX. *Indrani* Farms & Lands (IFL)
XXXI. *Indrani* Empires & States (IES)
XXXII. *Indrani* Marks & Trades (IMT)

## 9. References

Dehra, H. (2004). A Numerical and Experimental Study for Generation of Electric and Thermal Power with Photovoltaic Modules Embedded in Building Façade, submitted/unpublished Ph.D. thesis, Department of Building, Civil and Environmental Engineering, Concordia University, Montréal, Québec, August 2004.

Dehra, H. (2006). A 1-D/2-D Model for an Exterior HVAC Rectangular Duct with a Steady Solar Heat Flux Generation, orally presented at the proceedings of the Second International Green Energy Conference, Oshawa, Ontario, June 25-29 2006, 1240-1251, 0978123603.

Dehra, H. (2007a). The Effect of Heat and Thermal Storage Capacities of Photovoltaic Duct Wall on Co-Generation of Electric and Thermal Power, in the proceedings of American Institute of Chemical Engineers - AIChE 2007 Spring Meeting, Houston, Texas, USA, April 22-26, 2007, Session 36a.

Dehra, H. (2007b). On Solar Building Energy Devices, 18th IASTED International Conference on Modelling and Simulation, Montréal, Québec, May 30-June 1, 2007, 96-101, 9780889866645.

Dehra, H. (2007c). A Unified Theory for Stresses and Oscillations, Canadian Acoustics, (September 2007), Vol. 35, 3, 132-133, 07116659.

Dehra, H. (2007d). Mathematical Analysis of a Solar Thermosyphon, International conference on Advances in Energy Research, Department of Energy Science and Engineering, Indian Institute of Technology, Bombay, December 2007, Macmillan, USA, 023063432X.

Dehra, H. (2008a). The Entropy Matrix Generated Exergy Model for a Photovoltaic Heat Exchanger under Critical Operating Conditions, International Journal of Exergy, Vol. 5, Issue 2, 2008, 132-149, 17428297.

Dehra, H. (2008b). The Noise Scales and their Units, Canadian Acoustics, 36, 3, (September 2008) 78-79, 07116659.

Dehra, H. (2009). A Two Dimensional Thermal Network Model for a Photovoltaic Solar Wall, Solar. Energy, Vol. 83, Issue 11, (November 2009) 1933-1942, 0038092X.

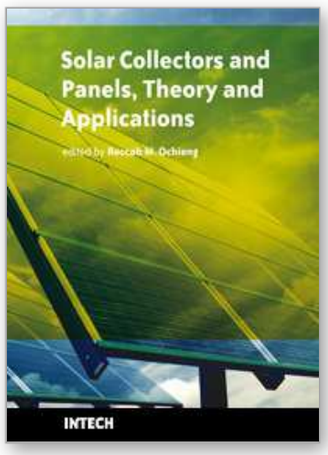


**Solar Collectors and Panels, Theory and Applications**

Edited by Dr. Reccab Manyala

ISBN 978-953-307-142-8
Hard cover, 444 pages
**Publisher** Sciyo
**Published online** 05, October, 2010
**Published in print edition** October, 2010

This book provides a quick read for experts, researchers as well as novices in the field of solar collectors and panels research, technology, applications, theory and trends in research. It covers the use of solar panels applications in detail, ranging from lighting to use in solar vehicles.

**How to reference**

In order to correctly reference this scholarly work, feel free to copy and paste the following:

Himanshu Dehra (2010). Solar Energy Absorbers, Solar Collectors and Panels, Theory and Applications, Dr. Reccab Manyala (Ed.), ISBN: 978-953-307-142-8, InTech, Available from: http://www.intechopen.com/books/solar-collectors-and-panels--theory-and-applications/solar-energy-absorbers

INTECH
open science | open minds

**InTech Europe**
University Campus STeP Ri
Slavka Krautzeka 83/A
51000 Rijeka, Croatia
Phone: +385 (51) 770 447
Fax: +385 (51) 686 166
www.intechopen.com

**InTech China**
Unit 405, Office Block, Hotel Equatorial Shanghai
No.65, Yan An Road (West), Shanghai, 200040, China
中国上海市延安西路65号上海国际贵都大饭店办公楼405单元
Phone: +86-21-62489820
Fax: +86-21-62489821

IntechOpen